Controlling bubbles

2003 J. Phys.: Condens. Matter 15 S415

(http://iopscience.iop.org/0953-8984/15/1/357)

INSTITUTE OF PHYSICS PUBLISHING JOURNAL OF PHYSICS: CONDENSED MATTER

J. Phys.: Condens. Matter **15** (2003) S415–S420 PII: S0953-8984(03)55141-4

Controlling bubbles

Detlef Lohse and Andrea Prosperetti[1]

Department of Applied Physics and J M Burgers Centre for Fluid Dynamics, University of Twente, PO Box 217, 7500 AE Enschede, The Netherlands

E-mail: lohse@tn.utwente.nl

Received 23 October 2002
Published 16 December 2002
Online at stacks.iop.org/JPhysCM/15/S415

Abstract

In this short overview we report on our ongoing work on the dynamics of bubbles in various flows. Three different situations are explored: the competition between acoustic and hydrodynamics forces in a vertical pipe (Rensen J, Bosman D, Magnaudet J, Ohl C D, Prosperetti A, Tögel R, Versluis M and Lohse D 2001 *Phys. Rev. Lett.* **86** 4819), a rising bubble on which shape oscillations have been induced (de Vries J, Luther S and Lohse D 2002 *Eur. J. Phys.* B **29** 503), and a bubble in a rotating horizontal cylinder. Whereas for the first two situations the standard bubble force models (Magnaudet J and Eames I 2000 *Annu. Rev. Fluid Mech.* **32** 659) are consistent with our measurements, modifications for the lift force model seem to be required in the last case.

1. Introduction

It is often desirable to control the motion of bubbles in flows. Examples include the application of bubbles in microfluidics for pumping and efficient mixing. Another example is bubbles in a medical context. While bubbles have long been used for ultrasound diagnostics [4], the focus now shifts towards their possible use in *therapy*, where they can act e.g. as vectors for directed drug delivery and gene transfection into living cells. It has been shown that the permeability of cell walls for large molecules (both drugs and genes) is dramatically increased in the presence of ultrasound and microbubbles [5]. As ultrasound can be focused onto specific areas and depths in the body, a localized therapy both through drug delivery and gene transfection may become possible, once the bubble motion can be controlled. A third example from application is two-phase flow in process technology, where the macroscopic flow behaviour as well as various gas–liquid exchange processes depend on bubble sizes and spatial distribution, which are in their turn affected by hydrodynamic forces.

A necessary condition for all these applications as well as many others is the understanding of the forces acting on bubbles. While some of these forces, such as buoyancy, are trivial,

[1] Permanent address: Department of Mechanical Engineering, The Johns Hopkins University, Baltimore, MD 21218, USA.

others are imperfectly understood. This in particular holds for the lift force: usually, it is assumed that the lift force coefficient C_L is constant for large Reynolds numbers, namely, $C_L = 1/2$ [3]. However, some experiments [6] suggest much larger values and a fourth-root dependence on the local vorticity.

It is therefore important to test the existing bubble force models against well-controlled experiments in order to resolve these and other uncertainties. In this short overview, we report on ongoing work and present three situations which are suited for this purpose (section 3). But first the bubble forces are introduced in section 2. Section 4 presents conclusions and gives an outlook on the consequences of the bubble forces for bubbly turbulence.

2. Forces on bubbles

An excellent recent summary on the present understanding of the forces on bubbles is given by Magnaudet and Eames [3]. An older standard reference is the book by Clift *et al* [7]. For a spherical bubble of radius R_B and volume V_B in a flow field $\boldsymbol{U}(\boldsymbol{x}, t)$ of constant density ρ_l these forces are [3]: the buoyancy force $\boldsymbol{F}_B = \rho_l V_B \boldsymbol{g}$, the drag force

$$\boldsymbol{F}_D = \tfrac{1}{2}\rho_l C_D \pi R_B^2 |\boldsymbol{U} - \dot{\boldsymbol{x}}_B|(\boldsymbol{U} - \dot{\boldsymbol{x}}_B), \tag{1}$$

the lift force

$$\boldsymbol{F}_L = C_L \rho_l V_B (\boldsymbol{U} - \dot{\boldsymbol{x}}_B) \times (\boldsymbol{\nabla} \times \boldsymbol{U}), \tag{2}$$

and the sum of added mass and inertial force

$$\boldsymbol{F}_A = \rho_l (C_M + 1) V_B \frac{\mathrm{D}\boldsymbol{U}}{\mathrm{D}t} - \rho_l C_M V_B \ddot{\boldsymbol{x}}_B. \tag{3}$$

Here $\boldsymbol{x}_B(t)$ is the position of the bubble and C_D, C_L, and C_M are the drag, lift, and added mass coefficients, respectively. The drag coefficient can be modelled as [3] $C_D = \frac{16}{Re}\{1 + \left[\frac{8}{Re} + \frac{1}{2}(1 + 3.315Re^{-1/2})\right]^{-1}\}$; the Reynolds number is $Re = 2R_B|\boldsymbol{U} - \dot{\boldsymbol{x}}_B|/\nu$. The added mass coefficient is $C_M = 1/2$ independently of Re [3]. The lift coefficient is the most controversial one. Typically it is assumed that $C_L = 1/2$, which holds for inviscid weak shear flow [3], but the aim of our work is to carefully test this assumption and equation (2) through experiment. Finally, there is the Basset history force, which however only contributes under certain conditions [3].

Newton's second law requires

$$\sum \boldsymbol{F} = \boldsymbol{F}_B + \boldsymbol{F}_D(\boldsymbol{x}_B, \dot{\boldsymbol{x}}_B) + \boldsymbol{F}_L(\boldsymbol{x}_B, \dot{\boldsymbol{x}}_B) + \boldsymbol{F}_A(\boldsymbol{x}_B, \ddot{\boldsymbol{x}}_B) = \frac{\mathrm{d}}{\mathrm{d}t}(\rho_g V_B \dot{\boldsymbol{x}}_B) \approx 0. \tag{4}$$

The last approximation holds as the gas density ρ_g is much smaller than the liquid density ρ_l.

It should be noted that, in a general flow field, the liquid velocity $\boldsymbol{U}(\boldsymbol{x}, t)$ will vary over the region occupied by the bubble. In writing the previous expressions we have assumed that any such variation is small enough to be negligible, so $\boldsymbol{U}$ can be evaluated at the bubble position $\boldsymbol{x}_B$. With this specification, equation (4) is a second-order ODE for the bubble path in the flow field $\boldsymbol{U}(\boldsymbol{x}, t)$ which can be solved straightforwardly. In the next section we will study three examples and compare the bubble trajectories with experimental results.

3. Exploring three different flow situations

3.1. Competition between acoustic and hydrodynamics forces in a vertical pipe

The first example that we want to study is one in which we let the above hydrodynamic forces on a bubble in a vertical diffuser compete with an acoustic force; see [1] for the full experimental

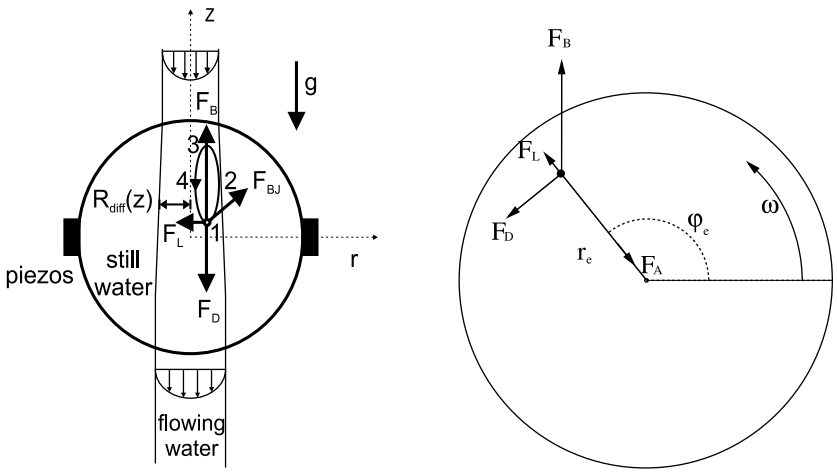

Figure 1. Left: the set-up used to study the competition between hydrodynamic and acoustic forces (section 3.1). The pressure antinode is at the very centre of the spherical flask. The relevant forces on the bubble are drawn in. Right: the force balance for a bubble in a rotating horizontal cylinder (section 3.3).

set-up and figure 1 for a sketch of the test section. The acoustic force originates from a standing acoustic field:

$$P_{acoustic}(\boldsymbol{x}, t) = P_a \frac{\sin(k\sqrt{r^2+z^2})}{k\sqrt{r^2+z^2}} \sin(2\pi f t), \tag{5}$$

which is generated by some piezos. Here, P_a is the sound wave amplitude, $f = 20$ kHz the resonance frequency, k the corresponding wavevector, r the radial distance from the centreline of the diffuser, and z the height, measured from the plane with the pressure antinode. The acoustic force acting on the bubble in this situation—the so-called primary Bjerknes force—is

$$\boldsymbol{F}_{BJ}(\boldsymbol{x}, t) = -V_B \nabla P_{acoustic}(\boldsymbol{x}, t). \tag{6}$$

The (downward) velocity in the diffuser is approximately given by

$$U(r, z) = \frac{-2Q}{\pi R_{diff}^2(z)} \left(1 - \frac{r^2}{R_{diff}^2(z)}\right), \tag{7}$$

where $R_{diff}(z)$ is the radius of the diffuser at height z and Q the volume flow rate. The resulting experimental trajectory for a $R_0 = 200$ μm bubble is shown in figure 2: the bubble spirals in an r–z plane, either inwards or outwards, depending on the control parameters Q and P_a.

For the theoretical description, the Bjerknes force (6) is added to the above force balance (4) and the ODE is integrated. The resulting trajectory is shown in the same figure (figure 2). Again, it is a spiral with a similar spiralling rate (about 0.38 Hz in this case) and damping constant. The physics of the force competition is as follows (see figure 1, left). At '1' the Bjerknes force is most relevant and drives the bubble away from the centre as the bubble is larger than the resonance radius. At '2' buoyancy takes over. At '3' the lift force becomes stronger than the acoustic force and pushes the bubble back to the centre. Finally, at '4' the drag pulls the bubble back to the centre where the Bjerknes force again takes over. The final result is a spiralling trajectory.

Unfortunately, in our experiment [1] the precision in measuring R_0 and P_a was too low to allow for a real test of the various force model expressions above. All that can be said is that,

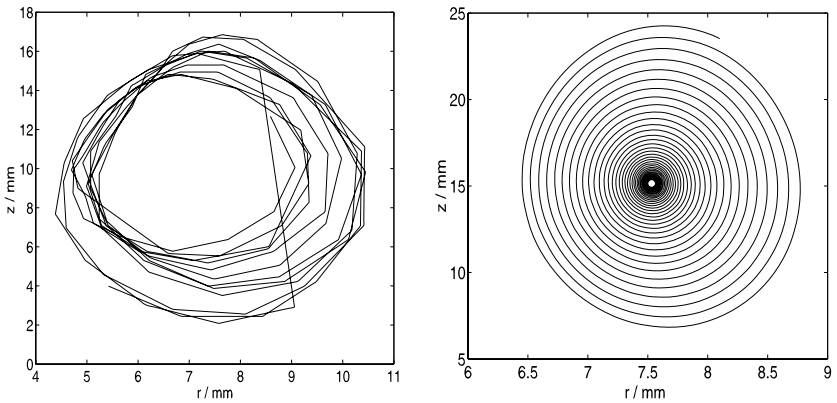

Figure 2. Left: experimental trajectory $r(t)$ versus $z(t)$ for $Q = 10^{-5}$ m^3 s^{-1}, $P_a \approx 4 \times 10^3$ Pa, and $R_0 = 200$ μm. The data are obtained with a digital camera operated at 25 Hz. The spiral is inwards. Right: the corresponding theoretical trajectory which is also an inwards spiral. (This figure was taken from [1].)

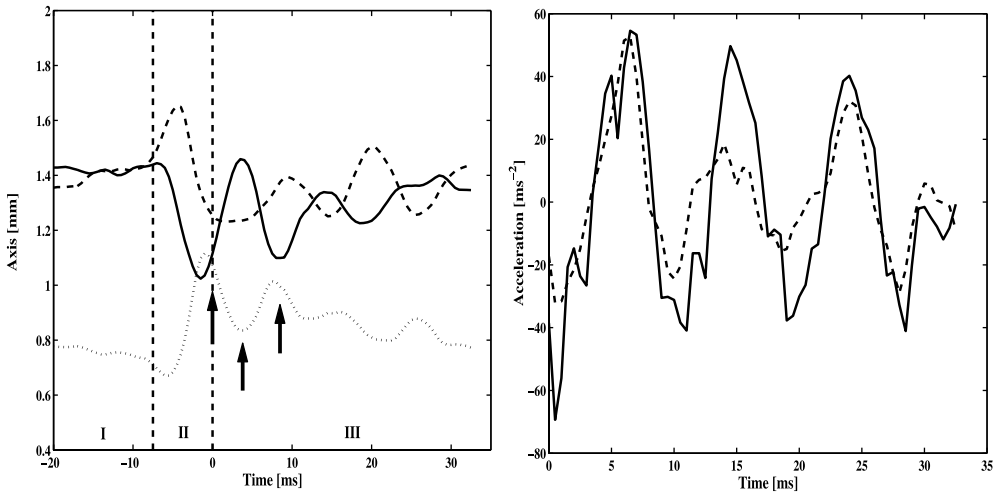

Figure 3. Left: experimental axes a and b (solid and dashed curves) and c (dotted curve) for a rising bubble before, while, and after hitting a thin wire. For $t < 10$ ms the bubble axes are constant within experimental errors. At $t = -7.5$ ms the interaction between the bubble and the hot-film probe starts. At $t = 0$ s the bubble detaches from the hot-film probe and its axes oscillate. The data are extracted from a high-speed digital video; the frame rate is 2 kHz. Right: the experimental (solid curve) and numerically calculated (dashed curve) acceleration of the bubble. (This figure was taken from [2].)

with those expressions, the experimental and theoretical results are consistent. More work to improve on the precision is in progress.

3.2. Forces on a rising shape-oscillating bubble

The second example is that of a rising bubble (with an ambient radius of $R_0 = 1.2$ mm) in still water which hits a 74 μm diameter wire. The collision induces shape oscillations, resulting in an oscillation of the bubble rise velocity (see [2] and figure 3).

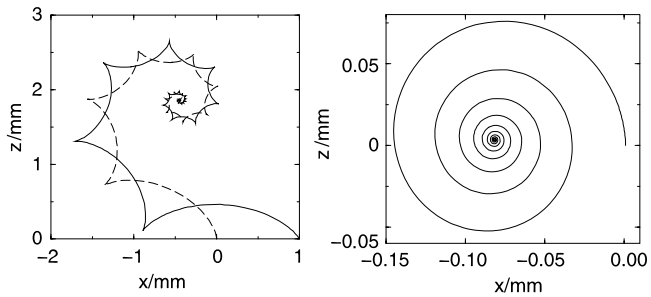

Figure 4. Inwards-spiralling bubble trajectories for a bubble in a horizontally rotating cylinder. $R_B = 5 \times 10^{-4}$ m, $\omega = 100\ \mathrm{s}^{-1}$, $\rho_l = 1000\ \mathrm{kg\ m}^{-3}$. In the left picture we have $\nu = 10^{-6}\ \mathrm{m}^2\ \mathrm{s}^{-1}$ and thus $Re_\omega = 4.17$; two different trajectories are shown. In the right picture $\nu = 10^{-4}\ \mathrm{m}^2\ \mathrm{s}^{-1}$ and thus $Re_\omega = 0.0417$.

For the theoretical description, as the water is still, we only have to consider the added mass force, the drag, and the buoyancy in the balance equation (4); the lift is zero. However, due to the shape oscillations, the added mass force and the drag force also oscillate. In [2] we show how to extend the force models correspondingly. The main result is that the rise velocity fluctuations originate from the oscillations in the added mass, not from those in the drag. A comparison between the experimental and the theoretical acceleration is shown in figure 3, right.

The conclusion from [2] again is that the existing force models are consistent with the experimental observation. However, for a detailed comparison, the precision of the data is again not high enough. A particular problem is that the bubble has already left the camera field of view just 30 ms after the collision, so no long-time behaviour could be studied. Moreover, the shape oscillations obviously complicate the checking of the force balances. Finally, the particularly controversial lift force is not relevant in this set-up.

3.3. Forces on a bubble in a rotating horizontal cylinder

So we move on to yet another geometry, namely a bubble in a horizontal cylinder rotating with angular velocity ω as previously studied in [8]. The local liquid velocity is then given by $U(r) = \omega r \boldsymbol{e}_\phi$. With this velocity field, the above force balance (4) is straightforwardly integrated. Examples of bubble trajectories are shown in figure 4. The advantage of this set-up is that the bubble approaches an equilibrium position which should be measurable with a higher precision than a trajectory. The force balance at the equilibrium position is shown in figure 1, right part. The equilibrium position has the cylindrical coordinates

$$\tan \phi_e = 2(2C_L - C_M - 1)Re_\omega = -Re_\omega \tag{8}$$

for $C_L = C_M = 1/2$ and

$$r_e = -\frac{g \sin \phi_e}{\omega^2(2C_L - C_M - 1)} = \frac{2g}{\omega^2} \sin \phi_e \tag{9}$$

for $C_L = C_M = 1/2$. Here, $Re_\omega \equiv R_B^2 \omega/(6\nu)$. Expressions (8), (9) allow for a direct measurement of $2C_L - C_M - 1$. Corresponding experiments are currently under way in our group. They will we hope enable us to precisely check in particular the lift force model (2). First results indicate that modifications of this model are required.

4. Conclusions

In conclusion, we can say that the force models of section 2 are consistent with our present experimental results. However, experiments on bubbles in the horizontal rotating cylinder are still ongoing. Of all experiments shown/suggested here, they potentially have the highest precision and, therefore, the potential for use in checking the expression (2) for the lift force.

The results on single bubbles have an important bearing on two-phase flow. The dynamics of point-like bubbles in turbulent flow is often modelled by the equation [9–11]

$$\frac{\mathrm{d}\boldsymbol{v}}{\mathrm{d}t} = 3\frac{\mathrm{D}\boldsymbol{U}}{\mathrm{D}t} + \frac{1}{\tau_b}(\boldsymbol{U}(\boldsymbol{y}(t),t) - \boldsymbol{v}(t)) - 2\boldsymbol{g} - (\boldsymbol{v}(t) - \boldsymbol{U}(\boldsymbol{y}(t),t)) \times \boldsymbol{\nabla} \times \boldsymbol{U}(\boldsymbol{y}(t),t), \quad (10)$$

where $\tau_b = R_B^2/6\nu$ is the timescale of the bubble in viscous flow [12]. Relation (10) is a direct consequence of the above force models with $C_M = C_L = 1/2$.

In [13] we have numerically shown that the dynamics (10), together with direct numerical simulations of the Navier–Stokes equations, lead to a bubble accumulation in vortices, but preferably on the downflow side. This is mainly an effect of the lift force and leads to a reduced average bubble rise velocity in a turbulent flow. Another consequence—once a back-reaction of the bubbles on the flow is allowed for—is a reduction of the downflow due to buoyancy and thus an attenuation of the turbulence on large scales [13].

Acknowledgments

We thank all of our collaborators on this subject, in particular St Luther, C D Ohl, J Rensen, and J de Vries. All experimental work was done by them. This work is part of the research program of FOM, which is financially supported by NWO.

References

[1] Rensen J, Bosman D, Magnaudet J, Ohl C D, Prosperetti A, Tögel R, Versluis M and Lohse D 2001 *Phys. Rev. Lett.* **86** 4819
[2] de Vries J, Luther S and Lohse D 2002 *Eur. J. Phys.* B **29** 503
[3] Magnaudet J and Eames I 2000 *Annu. Rev. Fluid Mech.* **32** 659
[4] Nanda N C and Schlief R (ed) 1996 *Advances in Echo Imaging Using Contrast Enhancement* 2nd edn (Dordrecht: Kluwer)
[5] Shohet R V *et al* 2000 *Circulation* **101** 2554
Blomley M J K *et al* 2001 *Biomed. J.* **322** 1222
Skyba D M *et al* 1998 *Circulation* **98** 290
[6] Sridhar G and Katz J 1995 *Phys. Fluids* **7** 389
[7] Clift R, Grace J R and Weber M E 1978 *Bubbles, Drops and Particles* (New York: Academic)
[8] Naciri A 1992 *PhD Thesis* University of Lyon
[9] Thomas N H, Auton T R, Sene K J and Hunt J C R 1984 *Gas Transfer at Water Surfaces* ed W Brutsaert and G H Jurka (Berlin: Reidel) p 255
[10] Spelt P D M and Biesheuvel A 1997 *J. Fluid Mech.* **336** 221
[11] Climent E and Magnaudet J 1999 *Phys. Rev. Lett.* **82** 4827
[12] Hadamard J 1911 *C. R. Acad. Sci., Paris* **152** 1735
Ribczynski W 1911 *Bull. Acad. Sci. Cracovie* **40** 40
[13] Mazzitelli I, Lohse D and Toschi F 2003 *Phys. Fluids* **15** at press